Hydrogen Embrittlement Behavior on Microalloyed Pipeline Steel in NS-4 Solution

A. Torres-Islas[1,], S. Serna[2], B. Campillo[3], J.Colin[1], A.Molina[2]*

[1]UAEM, Facultad de Ciencias Químicas e Ingeniería, PE. Ing. Mecánica, Av. Universidad 1001, Col. Chamilpa, 62209 Cuernavaca, Morelos, México
[2]UAEM, Centro de Investigación en Ingeniería y Ciencias aplicadas, Av. Universidad 1001, Col. Chamilpa, 62209 Cuernavaca, Morelos, México
[3]UNAM, Instituto de Ciencias Físicas / Facultad de Química, Av. Universidad s/n, Col. Chamilpa, 62209 Cuernavaca, Morelos, México
[*]E-mail: atimarquis93@yahoo.com.mx

Buried pipelines steels for oil and gas transport suffer near neutral pH SCC in their external surfaces. API (American Petroleum Institute) steel grades ranging from X52 to X100 were worldwide used that exhibit the classical ferrite + pearlite microstructures to complex constituent microstructures. Advances in alloy design technique and the adoption of new controlled rolling processes leads to a new generation of pipeline steel with higher strength and toughness. Fine-grained acicular and bainitic microstructures and most recently martensitic microstructures were developed by rapid cooling after controlled rolling**.** In the present work the hydrogen effects under stress as by products of the corrosion mechanisms in NS-4 solution, related to microstructural factors of a recently developed microalloyed pipeline steel were studied. Involving Polarization Curves (PC), Electrochemical Impedance Spectroscopy (EIS) and Slow Strain Rate Testing (SSRT). Hydrogen embrittlement cracking mechanisms were identified in both rolling directions. Some evidence seems to indicate that the HELP (Hydrogen Enhanced Local Plasticity) mechanism is present. This mechanism interacts with several steel ferrite types promoting hydrogen ingress minimizing their mechanical properties.

1. INTRODUCTION

Buried microalloyed pipeline steels integrity for oil and gas transport depends greatly on soil environment interactions. The choice of pipeline steel strength and microstructure would play also an important role to avoid catastrophic failures. Over the last three decades SCC was reported in several

countries throughout the world in buried, high pressure pipelines that constitutes a major failure of hydrocarbon transmission pipelines. This form of SCC occurred on outside surface of pipelines where the protective coating was disrupted and where be present a synergistic effect of coating, cathodic protection and soil. Most of these failures were intergranular [1-6], but in certain cases, such as in the Trans Canada Pipelines LTD, transgranular cracking have been observed . Since then, there has been a lot controversy about the transgranular stress corrosion cracking (TGSCC) that can develop in pipelines under normal operating conditions. There are major differences between the two forms of pipeline SCC. High pH SCC, engendered by concentrated bicarbonate or carbonate-bicarbonate solutions, has usually an intergranular morphology, and the cracks are sharp, with little lateral corrosion. Near neutral pH SCC, engendered by anaerobic, dilute ground water, has a transgranular, quasi-cleavage crack morphology with appreciable lateral corrosion of the crack sides. Field measurements in the vicinity of cracking indicate TGSCC is associated with a electrolyte with a pH in the range of ~6 to 7. This solution contained appreciable quantities of chloride, sulfate, as well as bicarbonate and very small amount of carbonate ions [1-6]. Based on the analysis of solutions from the initial failures, solution termed NS-1, NS-2, NS-3, and NS-4 were developed to simulate TGSCC environments in the laboratory. The range of compositions for these is potassium chloride, 40-150 mg/l, sodium bicarbonate, 480-1000 mg/l, calcium chloride, 10-180 mg/l, and magnesium sulfate, 90-250 mg/l. Most recently, NS-4 solution [7,8] appears to have become the favored "standard" environment for crack propagation experiments in most laboratories.

On the other hand, to control or prevent hydrogen embritlement due to NS-4 corrosion mechanism, environmental, metallurgical and mechanical factors should be considered. In general the lower strength steels are featured by high C content and ferrite/pearlite structures. While higher strength steels are typically pearlite reduced, low C steels produced in controlling rolling or thermomechanical controlled processing. The development of high strength pipeline steels is driven by the desire to reduce the construction cost of gas and oil transmission pipelines. An alternative to conventional pipeline steels such as API grades X52 and X65 was the development of X70 pipeline steel with 480 MPa of yield strength resistance. Lu [9] studied the relationship between yield strength and near-neutral pH SCC resistance of pipeline steels. He found that SCC resistance decreased with strength level but it was greatly affected by microstructure. Among concerns for the use of higher strength steels is the concern of hydrogen-induced stress cracking for this kind of pipeline steels. In this way many efforts have been made to understand the mechanism of this SCC in this non-classic environment [10-15].

The purpose of the present work was to study the hydrogen effects under stress as by products of the corrosion mechanisms in the NS-4 solution, related to microstructural factors of a recently developed microalloyed pipeline steel. For this purpose the NS-4 simulated ground water solution with pH 6.7, using electrochemical and the SSRT techniques.

2. EXPERIMENTAL PROCEDURES

The steel assessed was a modern microalloyed pipeline steel plate, with composition as specified in Table 1. The steel was fabricated by a metallurgical group of the Pittsburg University.

Conventional axial tension testing was carried out in the microalloyed steel plate, in the longitudinal and transverse rolling direction. The tension testing steel specimens were cut and machined according the ASTM E8 Standard using a Instron Universal test machine.

Table 1. Microalloyed steel chemical composition (wt%)

C	Mn	Si	P	S	Al	Nb	Cu	Cr	Ni	Mo	Ti	Fe
.0319	1.03	.2355	.003	.002	.052	.0235	.010	.424	1.30	.1674	.0149	Bal.

$1cm^3$ steel plate specimens were sliced and polished up to 1 μm diamond paste. After the last sequence of polishing, the specimen is rinsed with distilled water, cleaned with a soapy-water-soaked cloth, rinsed again, and flushed with ethanol. It is then dried under a warm air flow. This operation must be repeated several times to eliminate any trace of lubricant or impurities from the last polishing step. The steel polished surface was etched first with several etchants reported elsewhere [16], to elucidate the steel microstructure with Optical and Scanning Electron Microscopy.

For the SSRT test, cylindrical tensile specimens with a 25.00 mm gauge length and 2.50 mm gauge diameter were machined from the microalloyed pipeline steel plate in the longitudinal and transverse rolling direction. Before testing, the specimens were abraded longitudinally with 600-grade emery paper, degreased, and masked, with the exception of the gauge length. Specimens were subjected to monotonic slow strain rate tensile testing in dry air as an inert environment, and in NS-4 solution at room temperature with pH= 6.7 and a strain rate of 1.36×10^{-6} s^{-1}. Composition of NS-4 solution is specified in Table 2. Some specimens were pre-charged with hydrogen and strained to rupture either in air and NS-4 solution. The pre-charging with hydrogen was done in 0.5 M sulfuric acid (H_2SO_4) with a cathodic current density of $0.1mA/cm^2$ during 30 min. After charging inmediatly the samples were embebed into the cell, and then attached to the SSRT machine.

Table 2. NS4 test solution. Composition in gr/L

KCl	NaHCO$_3$	CaCl$_2$.2H$_2$O	MgSO$_4$.7H$_2$O
0.122	0.483	0.181	0.131

The loss in ductility was assessed in terms of the percentage area reduction (%RA) by using:

$$\%R.A. = \frac{A_i - A_f}{A_i} \times 100 \qquad (1)$$

Where A_i and A_f are the initial and final area respectively. The fracture surfaces were then examined using scanning electron microscopy (SEM).

Electrochemical cell arrangement were using three-electrode , with X70 steel electrode as working electrode, a saturated calomel electrode (SCE) as reference electrode and a graphite rod as counter electrode. The work electrode for electrochemical tests were embedded in epoxy resin leaving a working area of 1.0 cm^2 ,and preparation was carefully controlled to ensure that there was no grooving and bubble at the epoxy/steel interface. The working surface was subsequently polished with 800 grit and 1000 grit emery papers, cleaned by distilled water and methanol. Potentiodynamic polarization curves were performed at a sweep rate of 1.0 mV/s using a fully automated ACM potentiostat controlled with a desktop computer, and ACM Analysis v4 software. Before recording the polarization curves, the open-circuit potential was stable within 30 min. Additionally electrochemical impedance spectroscopy (EIS) test were done at frequency range of 10000 to 0.1 Hz. All potentials are referred to the saturated calomel electrode (SCE). The test solution was prepared from analytical grade reagents. Also, electrochemical polarization curves at fast and low sweep rates (0.1mV/s and 10mV/s) were obtained for the steel, using a Ag/AgCl reference electrode, at the same mentioned conditions.

Prior to each electrochemical and SSRT test, the solutions were purged with high-purity nitrogen gas for 4 h to remove oxygen. The gas flow was maintained throughout the test.

3. RESULTS

The recently developed microalloyed pipeline steel alloy design was based on previous trials and related experience as well as on available literature concerning interrelationship between chemical composition, processing conditions and resulting properties. Account has been taken of modern steel making technology and the ability to produce steel grades with very low interstitial contents and high cleanness. Some rolling mills are not equipped to carry out severe controlled rolling and some pipeline users are prejudiced against the use of extremely low finishing temperatures. Neither of these were incorporated or contemplated in the original design concept for the steel such that the moderate processing regimes gave rise to the "High Temperature Processing" (HTP) designation. Steel ingots were cut into slabs that were subsequently hot controlled rolled at a high temperature processing to produce 10.9 mm thicknesses steel plates. Finally, the plates were accelerated cooled to produce a complex steel plate microstructure showing some mechanical properties anisotropy with respect their rolling directions.

3.1. Microalloyed Steel Microstructure.

Figure 1a,b shows the microalloyed pipeline steel plate microstructure elucidated by light and electron microscopy techniques. Modern high strength microalloyed steels rather have complex microstructures and require a more complicated analysis and different metallographic methods. In spite of its simplicity, a etching procedure reported elsewhere [16] was applied to steel surface and has the advantage of allowing the simultaneous observation of the various phases that generally compose their complex microstructures, (i.e., bainite, polygonal and acicular ferrite, austenite, and martensite).

From figure 1a. it appreciate that acicular ferrite is present in the steel combined with some polygonal ferrite (gray zones). Figure 1a also shows the steel surface etched to preferential staining the different phases present in much lesser amounts such as: bainite and martensite (dark patches), and retained austenite (white zones).

For SEM tempered multiphase microstructures successful observation the specimen preparation with nital etching requires about 2s longer than the duration usually used for Light Microscopy microstructures. This is necessary to reveal the martensitic and bainitic grains internal substructure (dark zones in figure 1a) to allow their unequivocal recognition even when their size is very small (Fig. 1b), The emergence of the martensite substructure can be interpreted as resulting from carbide precipitation during tempering [17]. Because coarse particles precipitation occurs preferentially at interlath or interplate boundaries within low-carbon martensite grains [18], nital etching leads finally to the resolution of the martensite and bainite substructure, as shown in Fig. 1b. However the difference among this two microstructures is difficult to reveal their details, with this type of microscopy.
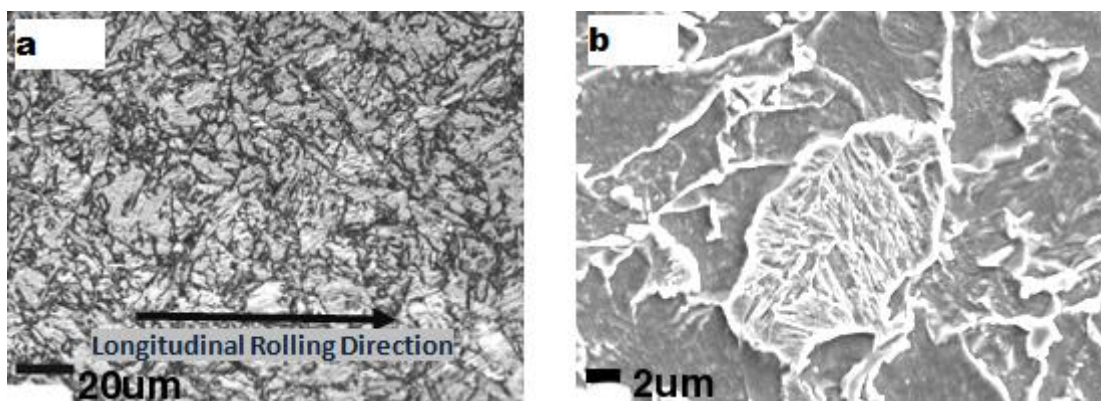
Figure 1. Microalloyed Pipeline Steel Plate Microstructure. a) Optical and b) SEM microphotographies.

3.2. Mechanical Properties

Table 3. Microalloyed steel mechanical properties

	YS (MPa)	UTS (MPa)	Elong (%)	Deformation (mm)	Rolling Direction
170.5	515	681	14.588	7.294	Longitudinal
163.35	501	663	14.132	7.066	Transversal

E= Young Modulus, YS = Yield Strength, UTS=Ultimate Tensile Strength, Elong= Elongation

Table 3 shows the results of uniaxial tension tests to the steel, in the longitudinal and transversal direction with respect to their rolling direction. As can be seen the mechanical properties in the steel longitudinal rolling direction were better compared with the steel transversal direction. Also,

the steel longitudinal rolling direction present more ductility but in this case the difference were not substantial.

The pipeline steel derived from this HTP concept was equivalent to a API X75 grade in the longitudinal direction, having a minimum yield strength level of 75 Ksi (515 MPa) along with high toughness in both rolling directions. With regard to toughness no specific target was set, rather the objective was to demonstrate what levels might be achieved in very clean steels if technically required for some application.

3.3. NS4 Solution hydrogen effect over the Electrochemical Tests.

Figure 2a illustrates the steel behavior in the potentiodynamic polarization test, as can be seen the corrosion potential (E_{corr}) was -224 mV_{SCE} and the i_{corr} obtained by the Tafel extrapolation method using only the anodic curve was of 0.2 mA/cm^2. In this case the E_{corr} value obtained is more anodic than other values reported in the specialized literature for these steels in contact with acid solutions, which fall in the -600 to - 400 mV_{SCE} range [19-21]. Regarding the obtained i_{corr} value this was increased by an order of magnitude.

On the other hand Figure 2b presents electrochemical EIS results on a Nyquist diagram; the impedance in the complex plane has the tendency to form a straight line with an angle of 45°.
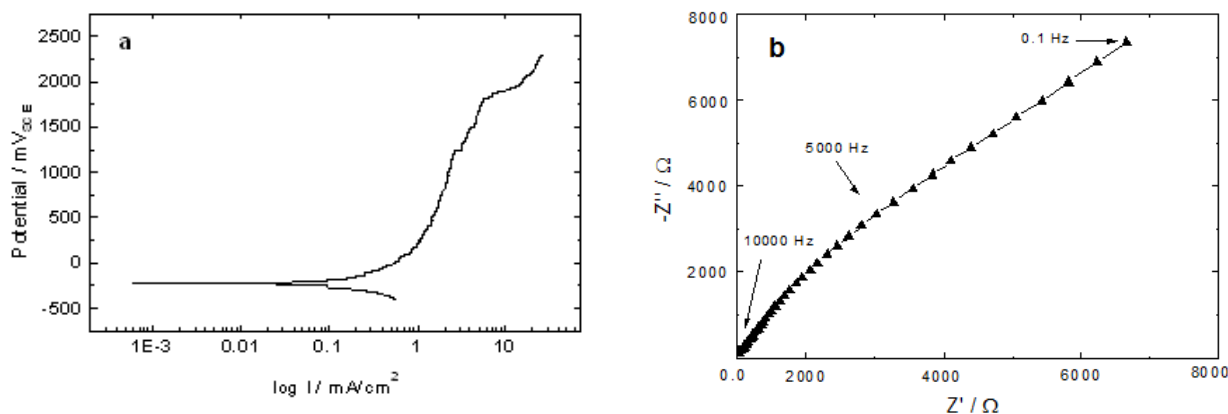
Figure 2. Electrochemical corrosion steel behavior in NS-4 test solution, (a)polarization curves and (b) EIS Nyquist plot.

This behavior indicates that there was mainly a diffusion mechanism on the surface of the steel. This fact is confirmed taking into consideration the asymptotic form of the polarization curve that is indicative of a continuous anodic dissolution. However the polarization in the anodic curve shows some variation in their continuity, this behavior is related eventually with the presence of a barrier between the metal and the solution. Although it is not a protective film, it affects the i_{corr}, as shown in the polarization curve at 1829 mV_{SCE} the i_{corr} increases suddenly which indicates that the barrier at this point suffers some type of damage or breakdown.

The potentiodynamic polarization curves of the steel in the test solution at slow and fast sweep rate are shown in Fig. 3. With the NS-4 solution, polarization curves at different potential sweep rates could show an active-passive transition over certain potential ranges, such transitions having been shown to be associated with SCC of ferritic steels. The location of that peak on the potential scale approximates to that in which cracking occurs, the indication of high anodic activity pointing to the formation of soluble corrosion products, while the current decay in the same region of potential is related with a film formation and thickening. SCC has correlation with pitting corrosion at initiation stage. The initiation of SCC and pitting is the result of the instability of the passive film. The technique was first proposed by Parkins [22] and can be used to forecast the different electrochemical process between non-crack tip area and the crack tip. First, the sample was polarized anodically at a fast scan rate of 10mV/s and then at a lower scanning rate of 0.1mV/s. The fast scan represents the behavior at crack tip, while the slow scan represents the behavior of side wall. At fast scan rate the steel has no sufficient time to reach a passive state, while at slow scan rate the steel could be passivated generating a corrosion film over its surface. The potential range where the fast and slow scan rate polarization curves exhibit large differences in current was identified as the SCC sensitive range [1]. As shown in Figure 3 for the fast and slow potential sweep rate curves of the steel in NS-4 solution the predictive potential range for SCC can occur is of 200 to -200mV$_{Ag/AgCl}$. (The -6mV difference in half-cell potential electrode in comparison with SCE, is not significant in present results analysis).
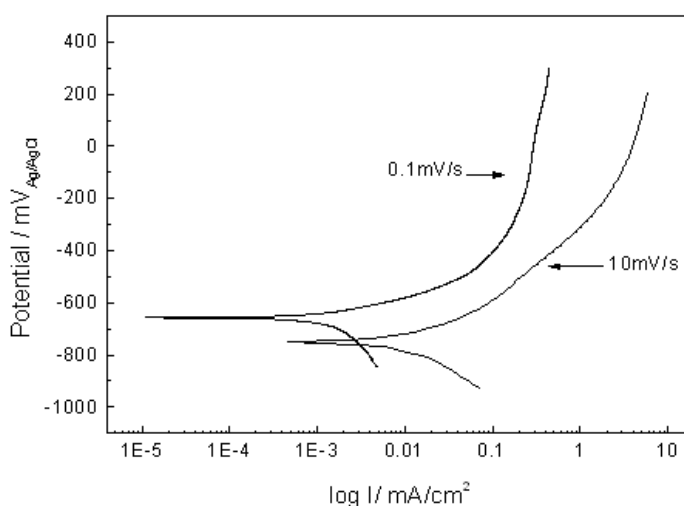

Figure 3. Microalloyed steel slow and fast sweep rates under NS-4 solution

However, for clarifying and study the SCC behavior susceptibility of steel microstructure under different conditions, different applied polarization potentials were plotted in Fig. 4. Each applied potential is corresponding to different electrochemical process according to both slow and fast rate sweep curves. For instance -600 mV$_{Ag/AgCl}$ is in the range of anodic reactions of both slow and fast rate sweep curves and -820 mV$_{Ag/AgCl}$ are both in the cathode range. For this Figure "if" and "is" are defined as fast and slow sweep current density respectively, and **(if - is)/is** was a normalized parameter

used to investigate SCC susceptibilities of the steel microstructure under the NS4 solution according to Parkins theory [22].
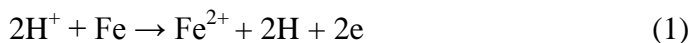
According to the results in Fig.4, (if -is)/is steel values at different potentials in the NS-4 solution conform approximately to a same tendence, with a difference that the value at -600 mV$_{Ag/AgCl}$ was higher than that of the other potentials. The values of (if-is)/is indicate that the electrochemical processes over steel surface were different at each polarization potential. Three points of interest can be related with crack tip and side wall processes. At -400 mV$_{Ag/AgCl}$ the value sign is positive but very close to zero, meaning that there is difference between crack tip and non crack-tip but both electrochemical processes are anodic [3]. When the potential is -600 mV$_{Ag/AgCl}$ reaches the higher positive value, meaning that the electrochemical reactions both inside and outside the crack tip are anodic too. At last when -820 mV$_{Ag/AgCl}$ is reached the value was positive and close to cero again, here the potential is in the cathodic side of the polarization curves. This can be due to that the electrochemistry is opposite in the crack tip and outside the crack, being the anode the crack tip and the cathode the side wall of the crack. So, it can be assumed that SCC mechanism of the steel in the NS-4 solution is anodic dissolution at -400 and -600 mV$_{Ag/AgCl}$, and a combination of anodic dissolution and hydrogen embrittlement at -820 mV$_{Ag/AgCl}$, mostly hydrogen embrittlement. The susceptibility of the steel to hydrogen steel could be explained as their microstructure as shown before was principally by a very fine acicular ferrite and small patches of bainite and martensite, which results in good toughness-high strength steel. As it well established as a rule of thumb that this kind of steels tend to be attacked by hydrogen embrittlement [23]. For this reason the original microstructure is prone to SCC as the applied potential drops from -600 to -820 mV$_{Ag/AgCl}$.
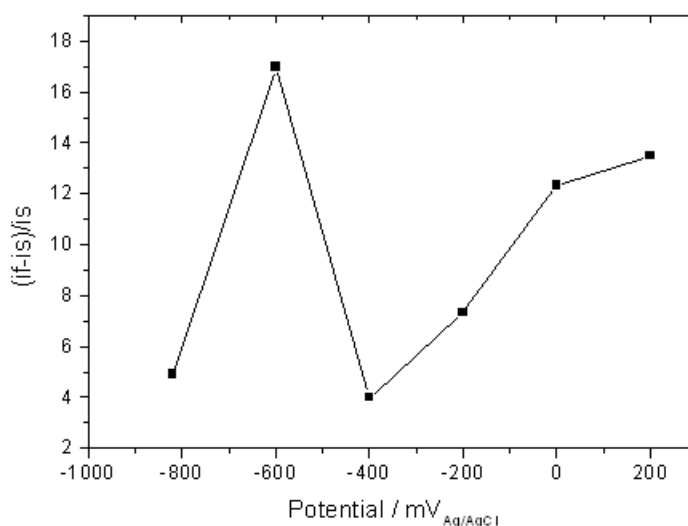
Figure 4. (if-is)/is values from the slow and fast sweep rates related to different polarization curves potentials

The source of hydrogen comes as a sub product due to the corrosion effect of solutions over steel crack tip or side wall crack tip. In the NS-4 solution the following ions could be present: HCO^{3-},

H_2CO_3 and H^+ all of these ions are important to SCC and hydrogen embrittlement according to literature [24]. H_2CO_3 comes from HCO^{3-} in acid environment. The NS-4 solution was oxygen free, so oxygen depolarization can be ignored and the electrochemical process could be described as follows:

$$2H^+ + Fe \rightarrow Fe^{2+} + 2H + 2e \qquad (1)$$

$$H_2CO_3 + e \rightarrow HCO^{3-} + H \qquad (2)$$

$$HCO_3^- + e \rightarrow CO^{2-}_3 + H \qquad (3)$$

These three process all proceed when pH<7, when -820 $mV_{Ag/agCl}$ is reached the cathode process is mainly de-oxidation of H^+ ion introduced by H_2CO_3 and HCO_3^-. The hydrogen proton (H^+) reduction process form atomic hydrogen (H) and speed-up hydrogen diffusion into steel matrix and micro crack sites. This can lead to localized hydrogen embrittlement in crack tip zones that will increase the steel susceptibility to fast rupture and cleavage fracture [25].

3.4. SSR Test

As seen in preceding sections, the steel has good mechanical properties comparable to a high strenght steel although a HTP process combined with accelerated cooling was involucrated to fabricate the microalloyed steel sheets. This processes can possibly leads to a steel microstructure susceptible to hydrogen embrittlement, and the test solution (NS-4 solution at a 6.7 pH) can evolve sufficient hydrogen to achieve the fragile cracking process as seen by analyzing Figures 3 and 4 data. On the other hand SCC by anodic process also can be present as showed by the slow and fast scan rates on Figure 3. However, to really elucidate the susceptibility of the microalloyed steels to SCC or Hydrogen embritllement in the presence of tensile stress, Slow Strain Rate test were carried out. As an attempt to simulate pipeline steel coating disbonding and rupture that is reported to form long wrinkles filled with ground water leading to severe solution conditions [26], some tensile samples were cathodically precharged with hydrogen and then tested with the NS-4 test solution. The test of the solely sample cathodicaly charged with hydrogen and then tested in air was maid for comparison to the samples charged with hydrogen and exposed to the NS-4 solution. The latter environment condition could match the conditions of the steel at $-820_{Ag/AgCl}$ as indicated in Figures 3 and 4 .

The effect of the hydrogen and the NS-4 solution on the reduction of area in SSRT testing is shown in Figure 5. The test conducted just in air (Air condition in Figure 5) serve as a reference area reduction parameter, which shows that the steel longitudinal and transversal to the rolling direction respectively, presented a ductile fracture. Under this conditions the area reduction is greater for the steel longitudinal rolling direction. This behavior was expected due to the more elongation value presented by the steel in this rolling direction. This means that although the strain rate is considerably less than for a conventional tensile test, the stress-strain curve shape is very similar for both tests: SSRT and conventional tensile test.
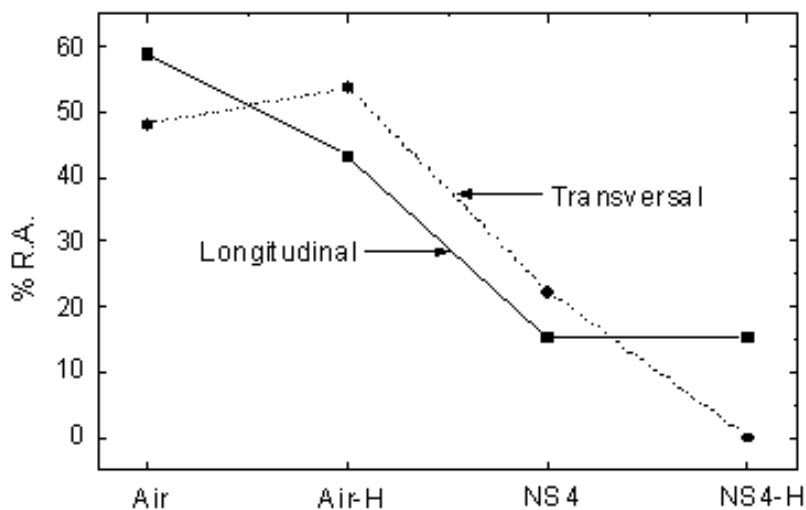
Figure 5. Steel performance under SSR test under different experimental conditions: Air, Air-H, NS4 and NS4-H.

In the hydrogen pre-charged tests (designated as Air-H in Figure 5) it can be seen that in both rolling directions a ductile fracture were evident with practical not cleavage fracture appearance as shown in Figure 6. However, in the longitudinal direction the steel was more susceptible to hydrogen embrittlement presenting a less area reduction.
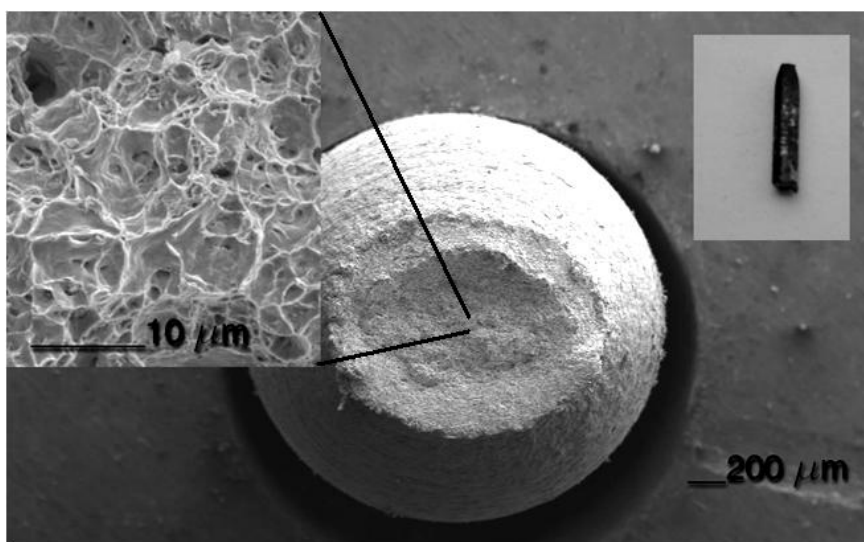

Figure 6. SSRT steel longitudinal specimens hydrogen precharged and fractured in air.

The hydrogen steel embrittlement could be due to small hydrogen quantities trapped in grain boundaries forming blisters. Some evidence of this embrittlement is shown in the steel fracture surface on Figure 6 where voids at grain boundaries and plastic deformation coexists. On the other hand in the

transversal rolling direction steel presented a slightly higher area reduction with respect the just in air reference tests indicating less suceptibility to hydrogen embrittlement. In addition the steel yield strength is lower (see Table 1) in the transversal rolling direction, which would eventually contribute to the less hydrogen effects in this rolling direction. Also in Figure 6 is observed in the right side insert the profile of one fractured part of the SSR steel test sample. It is shown at their tip a considerable area reduction as a consequence of the ductile behavior of the steel in the form of a cup. This test specimen profile is common to the longitudinal and transversal steel rolling direction tested either in air and with hydrogen precharging. So, as mentioned before, this steel is particularly resistent to hydrogen precharged effects.

Figure 5 shows that for steel in both rolling directions in the NS-4 solution the area reduction was significantly lower than in the previous conditions, with 15.3 and 22.4 % area reduction values for the steel longitudinal and transversal rolling direction respectively. In the rectangular left insert of Figure 7 is shown the inferior end of a fractured SSRT steel transversal specimen in the NS-4 solution, showing some necking. However, the fracture profile tend to form a 45 ° line with respect to stress application.
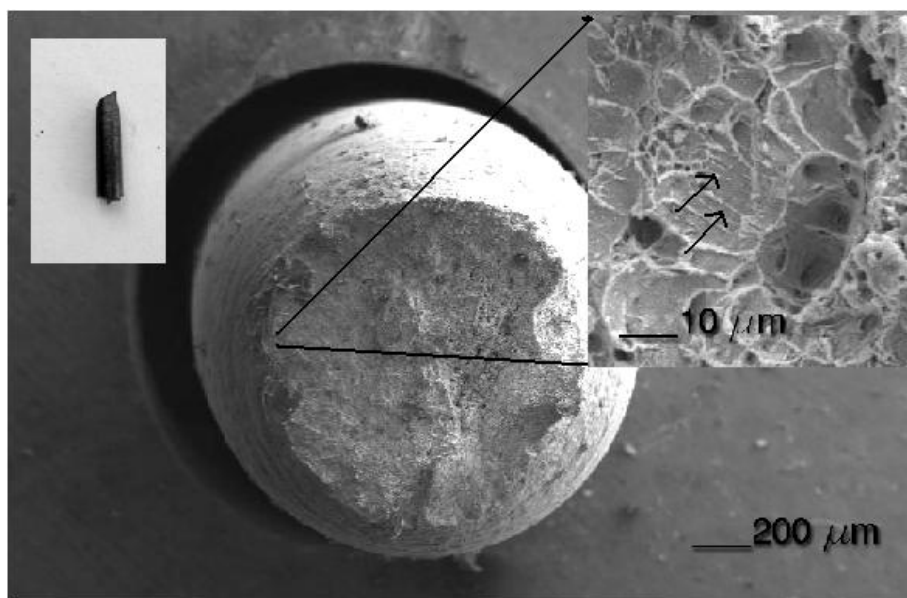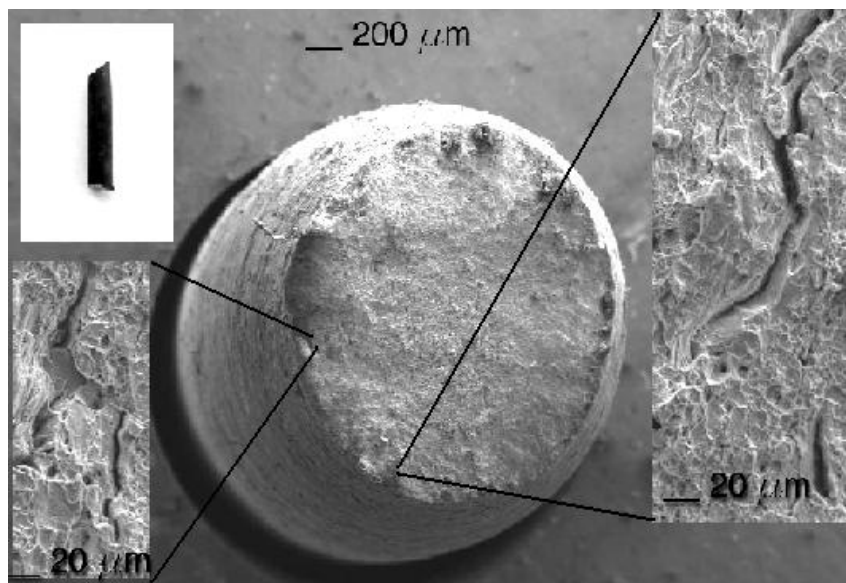

Figure 7. Steel SSRT transversal specimen fractured in NS-4 solution

The fracture surface, illustrated in the central part and right side insert of Figure 7, shows brittle fracture (cleavage planes) only at the border of the circular fractured sample indicated by the arrows. Also was appreciated in the right insert the coexistence of intergranular voids produced by hydrogen blisters.

On the other hand, there is no appreciable necking in the fractured steel longitudinal test specimens tested in the NS-4 solution, as shown in the left upper corner insert in Figure 8. There is only an 45 °angle with respect to the stress implementation. The fracture surface shows transgranular

cracks (left bottom and right inserts of Figure 8) located in the specimen fracture circular perimeter with lengths between 20 to 80 μm without visible inside corrosion products.

The SSRT steel logitudinal specimens precharged with hydrogen and exposed to NS-4 solution (NS4-H condition) shows a area reduction value with brittle fracture in the longitudinal direction of 15.3 % as seen in Figure 5. This value is equal to that obtained in the steel specimen in NS-4 solution without hydrogen precharge. However, the fracture surfaces of the steel specimens in the NS4-H solution exhibit two types of secondary cracks at their periphery (Figure 9).


**Figure 8.** Steel SSRT longitudinal specimen fractured in NS-4 solution

The first type are relatively large transgranular cracks without inner corrosion products as shown in the left box insert in Figure 9. The second type is related to lesser intergranular cracks with 10μm sizes, as shown by the ponting up arrow in the right bottom box insert of Figure 9. Also, there are signs of cleavage indicated by the pointing down arrow, and the profile of the fractured steel specimen (upper right box insert) presents a 45 ° pattern with respect to the tensile load application. For the transversal steel rolling direction in NS4-H SSR tests, the behavior was quite different.

The area reduction was insignificant, presenting a completely fragile fracture, with transgranular cracks in the sample periphery of the order of 200 μm, without the presence of corrosion products in its interior (right box insert in Figure 10). Cleavage planes were evident as indicated by the arrow in the left insert box (Figure 10). The steel sample test fractured profile (upper right insert on Figure 10) shows the same pattern as in previous cases of 45 ° with respect to the tensile load application.

On Figure 11 it shows a table with the electrochemical and SSRT test matrix.
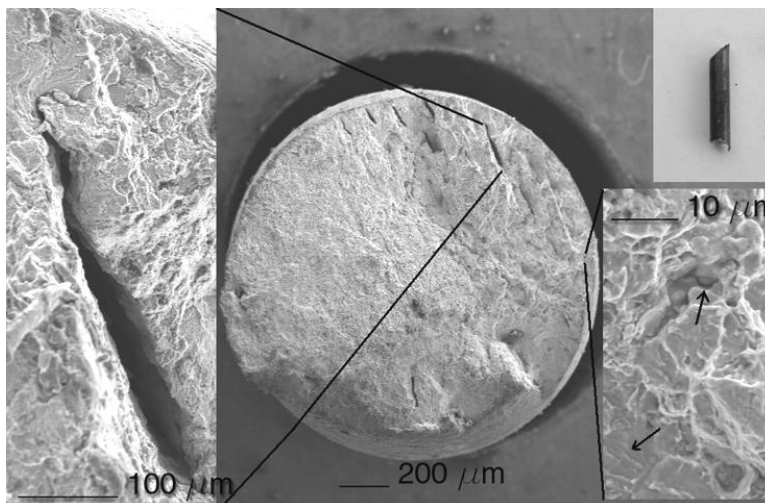
Figure 9. Fractography and steel sample test profile in the longitudinal direction at the NS4-H
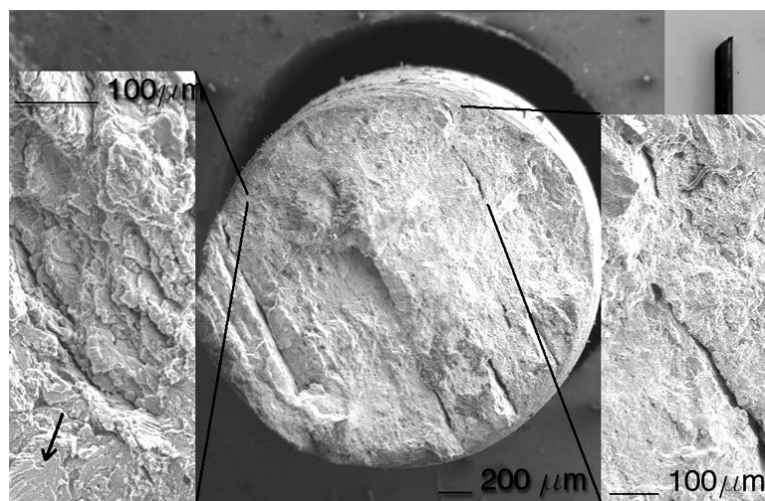
Figure 10. Fractography and steel sample test profile in the transversal direction at the NS4-H solution condition.

Figure 11. Table showing the electrochemical and SSRT test matrix.

4. DISCUSSION

Figure 5 show that in the Air and Air-H conditions regardless of the steel longitudinal or transversal direction, the microalloyed steel present a ductile fracture. On the other hand, in the NS-4 and NS4-H solutions the steel present fragile fracture in both rolling directions. These behaviors indicates that the test solution and the E_{corr} play an important role in the steel hydrogen embrittlement performance. Furtheremore, the hydrogen dissociation related to the steel deformation in a stress-strain field facilitates the penentration of the hydrogen to the steel crystal lattice [11]. The displacement of the E_{corr} to more positive values, point out that the cathodic reaction could be predominant before reaching equilibrium conditions. So, more hydrogen can be available to diffuse into the steel microstructure in the form of atomic hydrogen. The hydrogen diffusion thermodynamic behavior has been extensively reported,[11-15,19-27] finding invariably that the fracture mechanism and cracking susceptibility was directly related to crack tip anodic dissolution with passive film rupture generation, and hydrogen embrittlement. However, the polarizacion curve in Figure 1a indicates that steel corrosion behavior do not generate a passive layer in contact with the NS-4 solution and was dominated by the anodic dissolution mechanism.

As described before Air-H condition hydrogen does not generate significant embrittlement. Particularly in the transversal steel rolling direction present greater ductility with respect the longitudinal rolling direction. This behavior is most likely related to a mechanism known as Hydrogen-Enhanced Localized Plasticity (HELP) [28]. Such mechanism suggests that the stress level decreases due to the addition of hydrogen which promotes slip dislocations, leading to a failure caused by a ductile process. This behavior was illustrated by the fractography of Figure 6.

Due to the steel in the NS-4 solution not form a protective film (Figure 2a), the observed embrittlemnet was consequence of the hydrogen evolved during the corrosion process. For the transversal steel rolling direction case (Figure 7), the necking before fracture ocurrence was the result of the transition from a uni-axial stress to a tri-axial stress state due to localized plastic flow. Also, crack initiation at inclusion-matrix interfaces contribute to the necking behavior in the central sample region, then the fracture process continue by cracks propagating in radial form. The cracks begin propagating at central specimens locations towards the circular steel sample periphery, finally reaching the edge of the sample fracture surface [27]. Based on the previous behavior, particularly for this steel in the NS-4 solution, the hydrogen generated by corrosion process causes cracking by two complementary hydrogen mechanisms: HELP and the hydrogen embrittlement (HE) cracking mechanisms. So, at an early stage the plasticity was increased by hydrogen-dislocation interactions giving rise to a ductile behaviour. In a second stage the continuous entry of hydrogen eventually weakened and embrittle the steel atomic bonds in both rolling directions, leading to cleavage fracture and blisters as shown in Figures 7 and 8 respectively

Steel microstructure play an important role for the mehcanical behavior of the steel. The acicular like ferrite present in the steel (Figure 1a) have a caothic structure similar to that reported to the Widmanstätten ferrite [29], plus small amounts of bainite and martensite (dark patches) principally at grain boundaries (Fig 1a and 1b). These microstructural features contribute to increment the yield strenght and impose good toughness to the steel. The intrincsic steel strength and toughness produce a

vast strain field when a high stress is applied in both rolling directions as was the case in the SSR tests. This strain field seems to facilitate the hydrogen entry to the deformed steel lattice, making the steel more susceptible to hydrogen effects under the test environments assesed.

Respect to the corrosion steel behavior is well known that for pure iron a γ-Fe_2O_3 film is the responsible to the steel passivation [30-32], while a Fe_3O_4 layer promotes an oxidation state over the steel surface. Thus, the Fe_3O_4 layer don't contributes to disminish the steel anodic dissolution current. In addition, to get a real steel surface passivation state, first has to be formed a Fe_3O_4 corrosion products deposit, which in turn has a low oxidation state and is highly susceptible to chemical dissolution. That's why until the conditions necessary for the formation and relatively stabilization of this layer (Fe_3O_4) was present, the γ-Fe_2O_3s protective film could not be formed and the dissolution of the steel will continue as observed in Figure 2a. Particularly in this study, the displacement of the steel E_{corr} to more anodic values could be related to the previous mentioned corrosion mechanism. This statement could be explained on the characteristics of the acicular ferrite structure, in which the rapid cooling from high temperatures led to a ferrite chaotic growth with a needle like form pointing to random directions. This growth leads sharp elongated grains nucleating inside prior austenite grains (figure 1a). This type of ferrite microstructure tends to create galvanic couples with inclusions and precipitates rounding them that could slow down the ferrite corrosion rate, limiting the Fe_3O_4 formation and stabilization promoting the continuous corrosion of the steel. The grain boundary martensite and bainite present in the steel could enhance this behavior acting as more active anodic zones, restricting more the ferrite corrosion rate.

Higher steels grades, with more strength levels, are more susceptible to hydrogen embrittlement. This statement is in accordance with this study, being the steel longitudinal rolling direction more susceptible to cracking and hydrogen embrittlement than the transveral rolling direction, as shown in Figure 5. As illustrated before in Table 1 the steel longitudinal rolling direction has the better mechanical properties, thus applying higher stresses to the SSRT speciemens major strain field zones could be produced. These deformed zones promote the hydrogen entrance and interaction with the steel lattice and related defects as dislocations.

For the NS4-H the area reduction for the steel SSRT samples in the transversal direction was bigger than in the lonely NS-4 solution condition (without hydrogen precharge). The presence of transgranular cracks was evident in their fracture surfaces (Figure 10) without corrosion prouducts inside the cracks. This cracks apparently grow from the SSRT center specimen to their circular border. Theoretically, crack initiation could occur at any weak point since the given conditions of hydrogen precharge and diffusion were uniform along the radial direction of the SSRT steel samples. However, Figure 10 shows a linear and parallel crack growth pattern in the steel SSRT smaple surface. This seems to indicate that fracture initiation, specifically in this steel with given conditions, was in the center of the samples. The beginning of the specimen fracture at the center could be acomplished by slip–microstructure interactions due to the combination of two hydrogen mechanisms like HELP and hidrogen decohesion.These mechanisms seems to operate in hydrogen concentration zones like dislocations, inclusions-matrix intefaces, and grain boundaries known to be strong hydrogen trapping sites.

Finally in the steel longitudinal rolling direction, the area reduction remained unchanged with respect to the test without hydrogen preload, presenting transgranular cracks with the same pattern as in the steel transversal rolling direction (Figure 9). However, the presence of intergranular small cracks suggest that during the hydrogen difussion some remains trapped in grain boundaries with the absence of inside cracks corrosion products. The steel in its longitudinal rolling direction microstrucutre present more slightly elongated grains, with a extended area related to their grain boundaries. These grain boundaries being high energy sites have a greater affinity for hydrogen trapping, leading to a reduction in transgranular hydrogen blisters that eventually decreased its cracking susceptibility, compared to the steel transversal rolling direction cracking susceptibility.

5. CONCLUSIONS

The microalloyed steel under study mainly presents a ferritic microstructure with various morphologies (aciular, polygon etc.) and to a lesser extent bainite and martensite in grain boundaries. This microstructure was the result of hot controlled rolling designated as "High Temperature Processing" (HTP) and accelerated cooling, which gives the microalloyed steel plate different mechanical properties with respect to their rolling directions. The steel in its longitudinal rolling direction enclose better mechanical properties, mainly with respect to its yield strenght, UTS and Young Modulus.

SSRT testing in both steel rolling directions shows that the microalloyed steel is susceptible to interact with the hydrogen, either pre-charged or produced by corrosion in the NS-4 solution, and their combination identified as NS4-H condition (hydrogen pre-charged + NS-4 solution). The latter condition simulates the hydrogen that can enter to the steel being cathodically protected where the protective steel coating has suffered a rupture. Microalloyed steel was susceptible in both rolling directions to SCC in NS-4 solution mainly by anodic dissolution and hydrogen embrittlement mechanisms, with the possible presence of the HELP mechanism too. The NS4-H test condition shows the same mechanisms but hydrogen embrittlement was increased, this was noted by the minor area reductions in the steel SSRT samples in both rolling directions.

The E_{corr} in the particular case of this steel under the solution conditions assessed was more anodic with regard to that reported in the literature. This result suggest that this behavior is closely related to the coexistence of different ferrite morphologies in the steel mainly related to the acicular ferrite with bainite and martensite patches at grain boundaries. This type of ferrite microstructure tends to create galvanic couples with inclusions and precipitates rounding them that could slow down the ferrite corrosion rate. Thus, limiting the formation and stabilization of the Fe_3O_4 leading to the continuous corrosion of the steel. The grain boundary martensite and bainite present in the steel could enhance this behavior acting as more active anodic zones, restricting more the ferrite corrosion rate.

It was also determined that this microstructure promotes a synergistic relationship between the hydrogen diffusion in the steel and their mechanical properties reduction. This was especially enhanced with respect to steel ductility loose indicated by their area reduction parameter in the NS-4 and NS4-H testing conditions, and the presence of cleavage characteristics in their fracture surfaces.

References

1. R.N.Parkins, "A Review of Stress Corrosion Cracking of High Pressure Gas Pipelines" Corrosion/2000, Paper No. 00363 (Houston, TX: NACE International, 2000)
2. B. Delanty, O'Beirne, *J.Oil Gas J,* 90 (1992) 39
3. B. Gu, W.Z.Yu, J.L. Luo, X. Mao, *Corrosion,* 55 (1999) 312
4. E.A. Charles, R.N. Parkins, *Corrosion,* 51 (1995) 518
5. R.R.Fessier, K.Krist, Research Challenges Regarding Stress Corrosion Cracking of Pipelines Corrosion/2000, Paper No. 00370 (Houston, TX: NACE International, 2000).
6. R.N. Parkins, "A Review of Stress Corrosion Cracking of Pipelines in Contact with Near-Neutral (Low) pH Solutions" Report PR -232-9701, Pipeline Research Committee Intl. (1999)
7. P. Andrews, M. McQueen, N. Millwood, *Corrosion,* 57 (2001) 721
8. A. Benmoussa, M. Hadjel, M.Traisnel, *Mater Corros,* 57 (2006) 771
9. B.T. Lu, J.L. Luo, *Corrosion,* 62 (2006) 129
10. Y.F. Cheng, *Int. J. Hydrogen Energy*, 32 (2007) 1269
11. Y.F. Cheng, *J. Mater. Sci*. 42 (2007) 2701
12. G. Van Boven, W. Chen, R. Rogge, *Acta Mate,.* 55 (2007) 29
13. W. Chen, G. Van Boven, Rogge R, *Acta Mater*, 55 (2007) 43
14. B.Y. Fang, E.H. Han, J.Q. Wang, W.Ke, *Corros. Eng. Sci. Tech*, 42 (2007) 123
15. B.Fang, E.H. Han, J. Wang, W. Ke, *Corrosion,* 63 (2007) 419
16. F. S. LePera, *J. Metall,* 32 (1980) 38
17. G. R. Speich and K. A. Taylor, *Tempering of ferrous martensites In Martensite*, Materials Park, OH, ASM International, (1992)
18. G. R. Speich and R. L. Miller, "Tempering of Ferrite-Martensite Steels"- Proceedings of Symposium on Fundamentals of Dual-Phase Steels, (Chicago, IL; 1981)
19. Z.Y. Liu, X.G. Li, C.W. Du, G.L. Zhai, Y.F. Cheng, *Corros. Sci,* 50 (2008) 2251
20. A. Torres-Islas, J.G. Gonzalez-Rodriguez, J .Uruchurtu, S. Serna, *Corros.Sci,* 50 (2008) 2831.
21. Liang Zhang, Li Xiaogang, Du Cuiwei, Yizhong Wang, *Mater. Design,* 30 (2009) 2259
22. R.N. Parkins, *Corros. Sci,* 20 (1980 147
23. J.G. Gonzalez-Rodriguez, M. Casales, V.M. Salinas-Bravo, J.L. Albarran, L. Martinez, *Corrosion,* 58 (2002) 584
24. S. Nesic, J. Postlethwaite, S. Olsen, *Corrosion*, 52 (1996) 280.
25. B. Gu, J.L. Luo, X. Mao, *Corrosion,* 55 (1999) 96
26. Eslami, *Corr. Sc,* 528 (2010) 3750
27. Maoqiu Wang, Eiji Akiyama, Kaneaki Tsuzaki, *Corros. Sci,* 49 (2007) 4081
28. H.K. Birnbaum *Mechanisms of Hydrogen Related Fracture of Metals Hydrogen Effects on Material Behavior,* The Minerals, Metals & Materials Society, (1990)
29. G.Z. Koval'chuck, V.N. Geichenko, V.N. Yarmosh, L.V. Podobedova, *Met. Sci. Heat Treat,* 21 (1979) 114
30. S. Szklarska-Smialowska, *Passivity of Metals* Princeton NJ: Electrochemical Society Corrosion, Monograph Series, (1978)
31. J.A. Bardwell, B. MacDougall, and M.J. Graham, *J. Electrochem. Soc,* 135 (1988) 413
32. J.L. Ord, D.J. DeSmet, *J. Electrochem. Soc,* 113 (1966) 1258